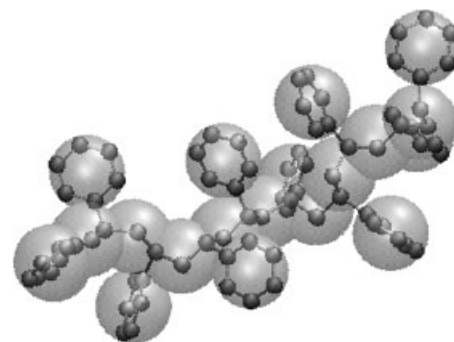


Comparison Between Coarse-Graining Models for Polymer Systems: Two Mapping Schemes for Polystyrene

Dedicated to H. W. Spiess on the occasion of his 65th birthday

Vagelis A. Harmandaris, Dirk Reith, Nico F. A. van der Vegt, Kurt Kremer*

We present a detailed study of a new, optimized coarse-grained (CG) model of polystyrene (PS) and compare it with a recently published one (Harmandaris et al., *Macromolecules* **2006**, *39*, 6708). By implementing a different mapping scheme, the new model, augmented with softer nonbonded interactions, better reproduces the local chain conformations and melt packing observed in atomistic simulations of atactic PS. Both models properly predict the bonded distributions and are capable of simulating different tacticities without needing sidegroups. Both CG models fit dynamic data from long atomistic simulations after determining the scale factor for the simulation time. Together with a rigorous back-mapping procedure from the mesoscopic to atomistic description, this opens up a very feasible way for generating very long atomistic trajectories.



Introduction

Polymers are characterized by a broad range of length and time scales.^[1,2] For this reason the development of coarse-grained (CG) particle based models is an active research field. By using such methods the length and time scales accessible by simulations can be increased by several orders of magnitude.^[3–5] A common approach to obtain CG molecular models is to merge groups of chemically connected atoms into “superatoms” and deriving the

effective, CG interaction potentials by averaging over the microscopic details of the atomistic models. Several different models and approaches have been proposed in the literature, varying in the degree of coarse-graining.^[6–22] For this work, we follow an ansatz, where intramolecular and intermolecular interactions are treated separately.^[6,7,12] In the past, this ansatz has proven to be rather robust and transferable. Moreover, a straightforward back-mapping scheme (reintroduction of the chemical details) can be executed because we stay close to the underlying atomistic length scale.

Polystyrene (PS) is one of the most common commercial polymers and probably the most widely studied amorphous polymer.^[2] For this reason different CG models for PS have been reported in the literature.^[12–19] Recently, we have developed a 2:1 CG model for PS (each PS monomer is described through two CG superatoms).^[12] This model can describe PS sequences with varying tacticities and has been tested and validated for a number of structural

V. A. Harmandaris, D. Reith, N. F. A. van der Vegt, K. Kremer
Max-Planck-Institut für Polymerforschung, Ackermannweg 10,
Mainz 55128, Germany

E-mail: harmanda@mpip-mainz.mpg.de;
kremer@mpip-mainz.mpg.de; vdervegt@mpip-mainz.mpg.de
D. Reith

Fraunhofer-Institute for Algorithms and Scientific Computing,
Schloss Birlinghoven, St. Augustin 53754, Germany

and dynamical properties of atactic PS.^[12,22] Milano and Müller-Plathe studied the structural properties of PS by CG simulations using a 1:1 model, where superatoms are centered on the methylene carbons of two different types according to the diad they belong to.^[13] Sun and Faller focused on the dynamics of PS melts^[14,15] with a CG model in which one superatom centered on the carbon connecting the backbone with the side ring corresponds to a full styrene monomer. Because Sun's model uses a single superatom type it is applicable to atactic PS only.

The main purpose of the present work is to examine how the choice of two different, but closely related CG mapping schemes affects structural and dynamical properties of the simulated melt. This is important in general, since the mapping procedure is not unique but at the same time very crucial in terms of both efficiency and predicting power. Here we show that the new model is superior over a recently developed one. However, up to now we are only aware of one similar comparison applied to two different models for polycarbonate.^[7]

After a first short overview of the general CG procedure details of the simulations performed in this work, both atomistic and mesoscopic, are described in the CG Simulations of M2 and a comparison between the two CG models based on united atom simulations and experiment is presented in the Comparison of CG Models. Finally, our findings are summarized in the Conclusion.

Coarse-Graining Models

General Coarse-Graining Procedure

In the following, we give a short overview of the CG procedure in general. More details can be found elsewhere.^[6,7,12] The procedure starts by assuming that the total potential energy, U^{CG} , for a CG chain can be separated into two parts, i.e., a bonded part $U_{\text{bonded}}^{\text{CG}}$ and a nonbonded part $U_{\text{nonbonded}}^{\text{CG}}$

$$U^{\text{CG}} = \sum U_{\text{bonded}}^{\text{CG}} + \sum U_{\text{nonbonded}}^{\text{CG}} \quad (1)$$

The bonded interactions in the above equation are the potentials of mean force of the CG degrees of freedom (bond lengths, angles, dihedrals). They are obtained by sampling distribution functions P^{CG} from atomistic simulations of isolated polymer random walks. The whole methodology can be summarized in the following steps:

- 1) First, atomistic molecular dynamics (MD) or Monte Carlo simulations of isolated random walks are performed. These simulations should be performed using a force field determined by quantum-chemical methods to properly account for torsional barriers that greatly

affect the overall stiffness of the chain. At this stage we include only local interactions, additionally taking care that we avoid double counting when adding the intermolecular interactions to the CG force field later on. For MD a Langevin thermostat is needed to ensure proper equilibration.

- 2) Then histograms P^{CG} are sampled by collecting a large number of independent conformations for each PS random walk at a given temperature T . These probability distribution functions are, in general, unknown functions of the CG bond lengths, r , bending angles, θ , and dihedral angles, ϕ , i.e., $P^{\text{CG}}(r, \theta, \phi, T)$. A standard way to proceed,^[4-7] in order to calculate the CG force field parameters, is to assume that $P^{\text{CG}}(r, \theta, \phi, T)$ factorizes as

$$P^{\text{CG}}(r, \theta, \phi, T) = P^{\text{CG}}(r, T)P^{\text{CG}}(\theta, T)P^{\text{CG}}(\phi, T) \quad (2)$$

The assumption that the probability distribution function can be factorized is only valid if the internal CG degrees of freedom are uncorrelated. This has to be checked carefully and even abandoned, if the resulting correlations are too strong. In this respect, the choice of the CG mapping points is crucial.

- 3) Having the independent probability distributions, the CG bonded potentials are given from the inverse Boltzmann relations

$$U^{\text{CG}}(r, T) = -k_{\text{B}}T \ln P^{\text{CG}}(r, T) \quad (3)$$

$$U^{\text{CG}}(\theta, T) = -k_{\text{B}}T \ln P^{\text{CG}}(\theta, T) \quad (4)$$

$$U^{\text{CG}}(\phi, T) = -k_{\text{B}}T \ln P^{\text{CG}}(\phi, T) \quad (5)$$

It should be noted that in the above expressions the probability distribution functions for the bond length and bond angle are normalized by taking into account of the corresponding volume elements, namely, r^2 for bond length and $\sin(\theta)$ for the bending angle. Note also that by the above construction the CG potentials are temperature dependent.

- 4) Finally, the mesoscopic force field has to be completed by adding a suitable nonbonded interaction potential. Typical choices are Lennard-Jones-type potentials with heuristically modified exponents, or similarly modified WCA potentials (purely repulsive). This depends on the system and the intended use of the model.

New CG Model for PS

Recently, we have proposed a CG model for the study of PS melts in which one monomer of a PS chain is mapped onto

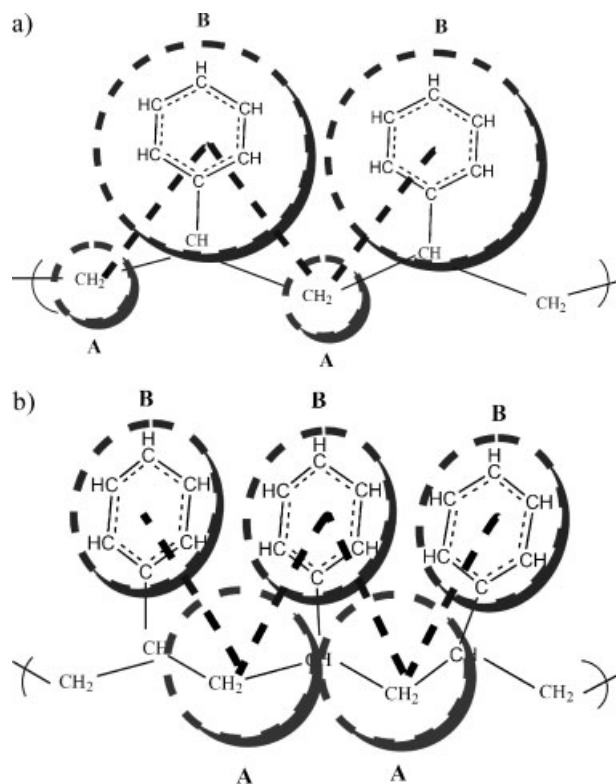


Figure 1. Two different coarse-graining mapping schemes of PS: (a) M1 model: mass ratio 1:6.5. (b) M2 model: mass ratio 1:2.8. Dashed lines show CG bonds between CG beads A and B.

two effective CG beads [see Figure 1(a)], i.e., a 2:1 model.^[12] In this model (from now on called M1) the CH₂ group of the backbone chain represents one CG effective bead (type “A”) whereas the remaining CH group of the monomer in the backbone and the phenyl ring are mapped to another effective CG bead (type “B”). This mapping scheme was chosen for keeping sufficient structural details (including tacticity) in comparison to the all atom system and at the same time to be fast enough in order to study the long time dynamics of polymer melts. M1 already had the advantage that there were no side groups at the CG level, i.e., the number of derived CG potentials was quite low. (In contrast, a CG model in which, e.g., the phenyl group would be represented as one CG side group, an improper dihedral potential would be required in order to keep the stereochemistry fixed.) Finally, it is relatively easy to develop a rigorous back-mapping procedure that reinserts all the atomistic details into the CG configurations, because typically small groups of covalently connected atoms (maximum around ten) are combined into a CG bead.

However, the large difference between the size (and relative mass) of the two CG beads: type A bead has a mass of only 14 amu whereas CG bead B has a mass of 90 amu, a

ratio of about 1:6.5 is of disadvantage. This asymmetry in size and/or mass has a strong effect for the dynamical behavior of the CG chains as will be shown in the next section. Similar effects have been observed for different systems by Marrink.^[21] If real masses are assigned to each CG bead, then for the fast motion of the bead A, a comparatively small time step must be used. (The steepness of the potentials would otherwise result in unrealistically large collision forces.) Despite this shortcoming, M1 has performed well for bulk PS^[12] and for a study of low molecular weight additives in PS.^[22]

To overcome these drawbacks, we propose a modified mapping scheme in which one PS monomer is also mapped onto two effective CG beads, but a CG bead A now includes information from three consequent CH_x groups along the backbone [see Figure 1(b)]. In this model (from now on called M2) CG bead A is the CH₂ of a PS monomer plus the half mass of each one of the two neighboring CH groups along the chain backbone, whereas CG bead B is just the phenyl ring. This keeps the advantage of capturing the tacticity without side groups, but in addition, it has a more suitable size and mass balance between the two beads; the mass ratio now is 1:2.8.

The whole methodology described in the previous section is now applied for the new CG model.^[12] Isolated random walk simulations of the united atom PS model are analyzed in the new CG description and the corresponding distribution functions, $P^{\text{CG}}(\phi)$, are obtained. We note that this procedure is performed with a completely isotactic as well as a completely syndiotactic sequence in order to obtain angle bending and dihedral torsion potentials for the meso- and racemic diad sequences present in atactic PS. As an example we plot in Figure 2(a) the probability distribution of dihedral angles, $P^{\text{CG}}(\phi)$, ($\phi = \text{ABAB}$ angle) for a racemic diad (SS) for the two mapping schemes. Clearly, $P^{\text{CG}}(\phi)$ of M2 has larger and sharper peaks than $P^{\text{CG}}(\phi)$ of M1. The corresponding dihedral potentials for the two mapping schemes are shown in Figure 2(b). Without going into more details, the rest of the CG bonded distributions show qualitatively the same picture. We finally point out that the CG model developed here applies to head-to-tail polymerized PS.

Concerning the nonbonded interaction, there are two important parameters that should be taken into consideration: the size of the beads and the “softness” of the potential. In our model there are two bead types and three different types of nonbonded interactions (A–A, B–B, A–B). In order to optimize the CG simulations for the dynamical properties, soft repulsive short-ranged potentials are used. At the same time, the melt structure should be reproduced as accurately as possible in order to reproduce structure and dynamics at length scales down to the size of the chemical repeat unit. This is achieved by using a generalized LJ-type nonbonded potential. Instead of the standard

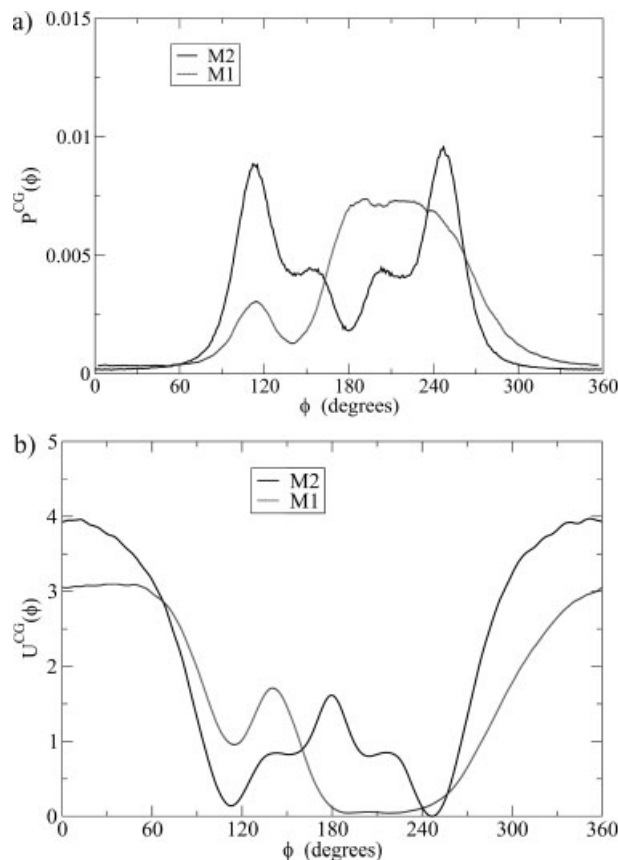


Figure 2. Dihedral (a) distributions and (b) potential of the ABAB/BABA angle of the SS racemic diad for the two different coarse-graining models. The distribution functions are smoothed prior to Boltzmann-inverting them to potentials in order to avoid singularities in the forces.

12-6 exponents, it is chosen to be of the form

$$U_{\text{NB}}^{\text{CG}}(r) = 4 \times \varepsilon [(\sigma_i/r)^{n_i} - (\sigma_i/r)^{m_i}] + U^{\text{shift}} \quad (6)$$

In this expression, σ_i describes the core size of the nonbonded interaction (A–A, A–B, or B–B) whereas n_i and m_i are power laws which determine the “softening” of the nonbonded potential. The term U^{shift} takes care that the potential minimum, which is at the cutoff, is shifted to zero. First the values of σ_i for A–A and B–B pairs are obtained from group contribution methods (bead A consists of one CH₂ and two half CH whereas bead B is benzene): we obtained $\sigma_A = 4.1 \text{ \AA}$ and $\sigma_B = 5.2 \text{ \AA}$.^[23] Due to the composite nature of the CG beads, all interactions should be described with a softer repulsive term than in the 12-6 LJ one. After fixing the σ_i in the above way, the exponents were varied manually to provide the best overall agreement between the bead–bead radial distribution function (RDF) of the CG melt and the correspondingly evaluated RDF of the atomistic melt [see Figure 6(b) and 7(b)]. A value of $n_i = 7.0$ (repulsive part) was found to be suitable for both “A–A”

Table 1. Values for the nonbonded parameters of Lennard–Jones-type potentials of model M2. The functional form is stated in Equation 6.

Interaction type	σ Å	n	m
A–A	4.10	7.0	6.0
A–B	4.65	7.0	5.0
B–B	5.20	7.0	4.0

and “B–B” interactions. For the power m_i the case is different. The standard power law of LJ, $m_{\text{A–A}} = 6.0$, is applicable for the A–A interaction, whereas a smaller exponent of $m_{\text{B–B}} = 4.0$ for the B–B interactions is found to reproduce the local packing of the B type CG beads properly. Finally, the “A–B” interaction is well described as a mix between the A–A and the B–B ones, i.e., $\sigma_{\text{AB}} = 4.65 \text{ \AA}$, $n_{\text{A–B}} = 7.0$ and $m_{\text{A–B}} = 5.0$. The values are summarized in Table 1. Note that in this model σ_A and σ_B were calculated through group contribution methods,^[24] in contrast with the model M1 where σ_B was calculated through the potential of mean force between two toluene molecules. The latter method, as we will see later, results into a slightly smaller value of σ . The strength of the potential is scaled with the temperature, i.e., $\varepsilon = k_B T$. Finally, the value U^{shift} , in kT units, is 0.2275 for A–A, 0.8115 for B–B, and 0.49235 for A–B interactions.

Correlation of Bending Angle and Dihedral Angle

As in most other CG studies, we make the basic assumption that all bonded potentials are decoupled and therefore bond stretching, bending angle and dihedral angle potentials can be determined [see Equation (2)] independently. In practice, however, this depends on the chemical structure of the polymer and the actual mapping scheme that is chosen. This means that even if there is a perfect matching between the CG and the atomistic representation for the individual bonded distributions, correlations between different distributions may be rather different. Because of that we here compare the decoupling assumption [see Equation (2)] for the two CG mapping schemes examined.

A direct way to check that is by plotting contour plots of combinations of energies (or probability distributions) of different bonded potentials in the CG description obtained from the united atom runs of the isolated PS fragments (random walks). For both models M1 and M2, the only interdependence between the bonded mesoscopic potentials is the one between the bond bending and dihedral CG angle. In order to examine this coupling effect more sys-

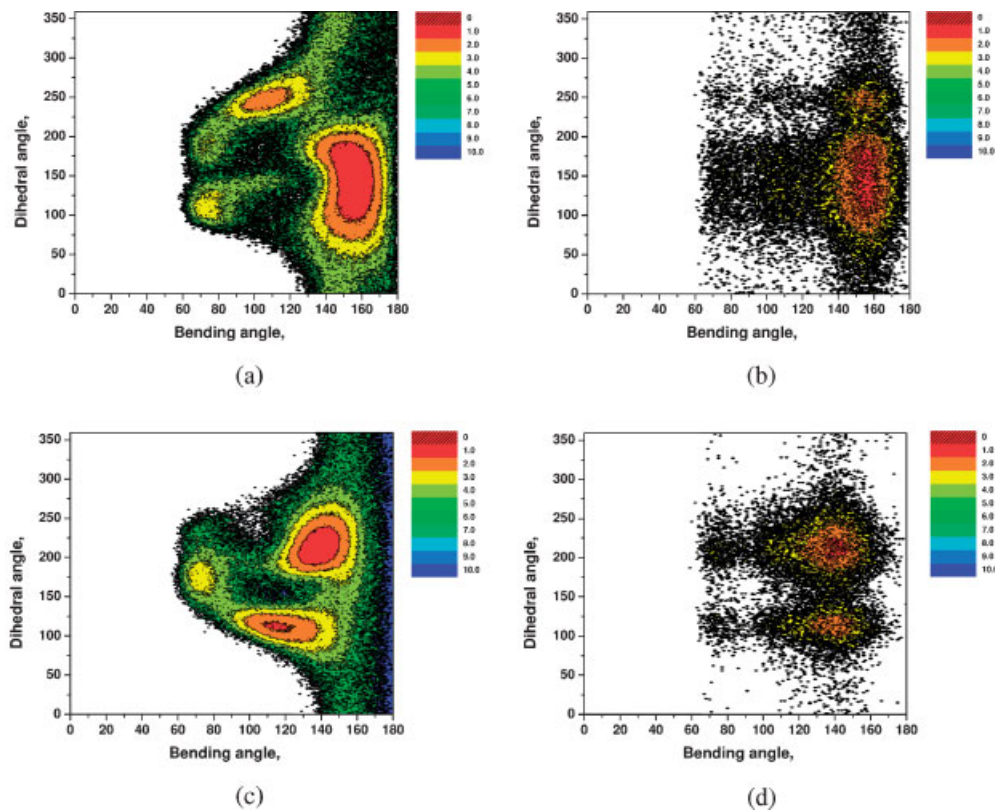


Figure 3. $(\theta-\phi)$ energy plot in the CG representation from the atomistic and the CG simulations for the racemic PS diad: (a) M1 atomistic data, (b) M1 CG data, (c) M2 atomistic data, and (d) M2 CG data. The energy units are in $k_B T$, $T = 463$ K.

tematically we choose the racemic sequence (i.e., syndiotactic position of the dihedral angles) for which the effect turns out to be more prominent than for the meso (or isotactic) case. The interdependence of the bending and the dihedral CG angles is shown in Figure 3(a)–3(d), which presents the energy surface plot $-k_B T \ln[P(\theta, \phi) / \sin \theta]$ of the CG dihedral angle versus the CG bending angle, i.e., a $(\theta-\phi)$ plot, for the racemic case at $T = 463$ K, obtained from the atomistic (united-atom model) and the CG simulations of the isolated PS dimers.

Figure 3(a) and 3(b) show the $(\theta-\phi)$ plot for the M1 mapping scheme obtained from the atomistic data (analyzed in the CG M1 description) and the CG simulations, respectively. From Figure 3(a), it can be seen that θ and ϕ are clearly correlated and that some regions of the angle–angle–surface are not populated at all. The comparison with the CG simulations, Figure 3(b), shows directly similarities but also some significant deviations. In both the atomistic and the CG models, the area of bending and dihedral angles sampled is roughly the same (i.e., bending angle from 60 to 180° and dihedral from 0 to 360°) and also the most favorable $(\theta-\phi)$ conformations (i.e., $\theta = 155^\circ$ and $\phi = 150^\circ$) are quite the same. At the same time, there are also some clear differences, the most important of which is that the second minimum in the atomistic simulations

($\theta = 100^\circ$ and $\phi = 250^\circ$) is found at much different θ angle at the CG runs, i.e., at $\theta = 155^\circ$. In addition an area in the $(\theta-\phi)$ plot, which is not allowed in the atomistic runs (e.g., $\theta = 80^\circ$ and $\phi = 50^\circ$), is sampled in the CG simulations. To exclude such conformations in the CG simulations, using the model M1, an additional 1–4 nonbonded repulsive interaction potential had to be taken into account. Such an adjustment after the parametrization step should be avoided, if possible, i.e., this is another shortcoming of the model M1. A more detailed analysis of the $(\theta-\phi)$ correlations can be found in our previous work.^[12]

The situation for the new mapping scheme M2 is clearly better as shown in Figure 3(c) and 3(d) for the atomistic data (analyzed in the CG description of the model M2) and CG data, respectively. Again the minimum in the $(\theta-\phi)$ plot is at the same point for both the atomistic and the CG simulations, i.e., $\theta = 140^\circ$ and $\phi = 200^\circ$. However, now we observe less differences between the two sets of data; the second minimum is almost at the same $(\theta-\phi)$ point ($\theta = 120^\circ$ for the atomistic data and $\theta = 140^\circ$ for the CG). In addition the not allowed region in the atomistic runs is sampled now much less frequently than in the case of the CG model M1. For this reason we do not need any additional 1–4 nonbonded potential. Note that the regions corresponding to $\theta = 170$ – 180° , which occur in the

atomistic but not in the CG description, are unimportant since these are sampled very rarely (energy $10 k_B T$) in the atomistic description. Overall, the new mapping scheme M2 reduces the information lost due to the assumption of decoupled bonded potentials, which is a direct advantage compared to the previous scheme.

CG Simulations of M2

All systems modeled by CG simulations of M2 in this study are presented in Table 2. Later on we will compare these to the same systems, simulated with model M1. In all cases, the chains are generated by an MC algorithm^[12,25] such that all the bond lengths, bending and dihedral angles of the CG chains follow the probability distributions of the corresponding atomistic simulation results. Additionally the 1–2, 1–3, and 1–4 nonbonded interactions are excluded since these interactions are described through the bonded potentials. For systems with MW from 20 kDa, only those initial random walks are accepted which satisfy an additional condition, i.e., $R^2(N) = C_\infty^{\text{CG}} N b^2 \pm 20\%$. This choice improves the starting configurations and is needed because of the small size of the simulated system (we have only 50 chains in the simulation box). In this expression, N is the number of beads along the backbone of a chain, i.e., $N = 2n_{\text{mon}}$ with n_{mon} the number of monomers, $R^2(N)$ is the square distance between monomers separated by N beads and b is the average bond length in the CG model M2, $b = 3.7 \text{ \AA}$ (note that for model M1 $b = 3.4 \text{ \AA}$). C_∞^{CG} is the characteristic ratio in the CG description calculated from the experimental value of C_∞ (for PS C_∞ is equal to 9.85^[26] at 300 K) corrected for the temperature difference (for PS $d \ln C_\infty / dT = -0.9 \times 10^{-3}$,^[26] so at $T = 463 \text{ K}$, $C_\infty = 8.0$) and by the bond length b . Using this condition we chose only those configurations with $C_\infty N b^2$ close to the mean value. This ensures that the internal distances at the time of generation of the polymers chain follow proper distributions for large N (MW above 5 kDa).

The CG chains are randomly placed in the cubic simulation box, thereby introducing significant local density fluctuations across the box. To decrease the density fluctuations, we perform a zero temperature Monte Carlo simulation in which two different moves (translation or rotation of a chain) are introduced. The density fluctuations are defined as $\langle \text{nbours}^2 \rangle - \langle \text{nbours} \rangle^2$ where nbours is the number of neighbors of the bead i within a radius of d ($d = 2\sigma$). Only those moves which lower the density fluctuations are accepted. In this stage, we do not change the single chain statistics which by construction have proper internal distances. More details of these MC algorithm can be found in ref.^[25] Note finally that in our CG simulations a polymer chain is of the form “ABA-BAB...AB”, i.e., it starts with a A and ends with a B bead.

MD simulations have been performed in dimensionless LJ units using m_A to scale all masses, $\sigma_{AV} = (\sigma_A + \sigma_B)/2$ to scale all lengths and $\epsilon = k_{BT}$ to scale all energies. By doing this a suitable unit of time τ can be defined as $\tau = \sqrt{m_A \sigma_{AV}^2 / \epsilon}$. The initially generated chains are still strongly violating the excluded volume constraints. To eliminate this effect, the intermolecular interaction potential is introduced slowly. In order to control the temperature in the system we use a Langevin thermostat with friction coefficient $\Gamma = 1.0 \tau^{-1}$. Once the bead overlap disappears we introduce full nonbonded interaction potentials to perform the MD simulations. One way to check whether the strong initial overlaps cause undesired conformational changes during the equilibration process is to analyze the internal distances $\langle R^2(N) \rangle$ of the chains. $\langle R^2(N) \rangle$ is the mean square distance between N CG beads along the polymer chain, i.e., for large values of N , $\langle R^2(N) \rangle$ approaches the end-to-end distance $\langle R^2 \rangle$. If $\langle R^2(N) \rangle$ approaches smoothly to $\langle R^2 \rangle$, then this is a clear evidence of well-equilibrated samples.^[25] Figure 4 presents the internal distances of the chains for the 10 kDa atactic PS melt, after a (longer) run of about 10 000 τ , for the two different CG mapping schemes. In the same graph the atomistic data for the short 1 kDa system are also given. For both models the graph shows no overshooting at small dis-

Table 2. Coarse-grained PS systems studied in the present work.

MW kDa	Number of beads per chain	Number of chains	Temperature K	Box size Å
1	20	480	463	94.96
2	40	240	463	94.31
3	60	160	463	94.09
5	96	100	463	93.70
10	192	50	463	93.62
20	384	50	463	117.8

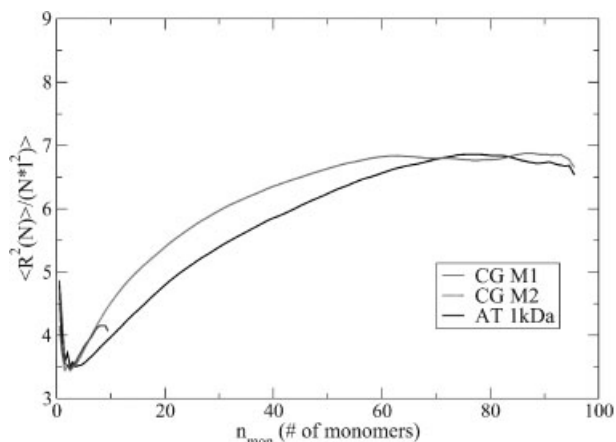


Figure 4. Internal distance distribution for the equilibrated configurations (run of about $10^4 \tau$) of a typical system (MW = 10 kDa) for the two CG models.

tances and hence equilibrated samples. Note again, that in Figure 4, the $\langle R^2(N) \rangle$ graphs are scaled with the number of bonds ($N = 2n_{\text{mon}}$). Also, the average atomistic bond length of the backbone bonds ($l = 1.53 \text{ \AA}$) is given in order to be compared with the experimental characteristic ratio, which is shown with dashed lines (with an error of 10%). Already here we observe significant improvements with the new model M2. More details about the generation and the equilibration of the polymer chains can be found elsewhere.^[12]

All CG MD simulations are performed using the ESPResSO package.^[27] The size of the box is fixed such that the density of PS melt is equal to that of the experimental density at the temperature studied. In CG models the bead friction is much weaker compared to atomistic systems. Therefore, a time mapping has to be incorporated in order to describe the dynamics correctly. In order to use a larger timestep, we have to assume that both CG beads have the same mass. This assumption cannot affect the structure of the CG systems, however, the dynamical properties will be influenced, as shown below. In order to analyze this, we perform also runs with the real mass ratios assigned to each bead and compare the difference in the dynamic properties (see next section). The time step used in the MD simulations was $\Delta t = 0.008 \tau$ for the model M1 and $\Delta t = 0.01 \tau$ for the M2 (the fact that the differences between the size the two CG beads are smaller for the new mapping scheme allows us to use a slightly larger time step in the integration of equations of motion). We perform MD simulations for times $\approx 10^4 - 5 \times 10^4 \tau$ depending upon the system size.

Finally, for the comparison of the two schemes, we reuse data from atomistic MD runs performed previously.^[12] In these simulations a UA model has been used

(the TraPPE model^[28]) and a number of systems with molecular weight up to 3 kDa has been studied. More details about the atomistic force field and the details of these simulations can be found elsewhere.^[12]

Comparison of CG Models

Static Properties

First, we investigate the characteristic ratio C_N , as shown in Figure 5, as a function of number of monomers, n_{mon} . In this graph there are data for both CG models as well as data for atomistic PS chains (up to 30 monomers) which were simulated for up to $0.3 \mu\text{s}$.^[12] The values of C_N for all datasets are in good agreement, within the error bars. Still, the agreement of the new model M2 is slightly better; the model M1 predicts a slightly smaller C_N value. The reason for this most probably is the rather small value of the B–B interaction in M1, which allows for a locally very tight packing. In the same graph we have also plotted the experimentally determined infinite characteristic ratio, C_∞ (dashed line with an error of 10%).^[26] As expected from theory, as the length of the PS chain is increasing, C_N approaches the limiting value predicted by the random coil hypothesis for the high molecular weight, C_∞ .

Direct information about structural features of the polymer systems can be obtained by inspecting the RDFs. Figure 6 and 7 show the curves as obtained from both the two CG models, and their comparison with the data from the atomistic simulations for the correlations between the CG beads, i.e., A–A and B–B, respectively. Note that in order to compare the two descriptions we analyze the atomistic RDFs at the level of the center of mass of the CG beads. In

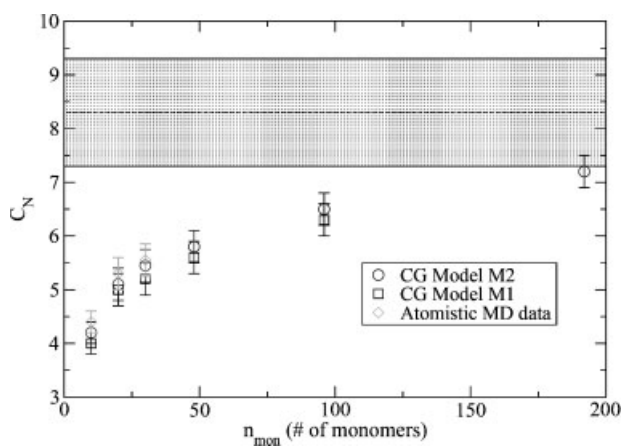


Figure 5. Dependence of the characteristic ratio on the number of monomers, obtained from the two different CG mapping schemes (circles and squares), atomistic simulations (diamonds), and experimental data (dash line) ($T = 463 \text{ K}$). Dash lines represent experimental values $\pm 10\%$.

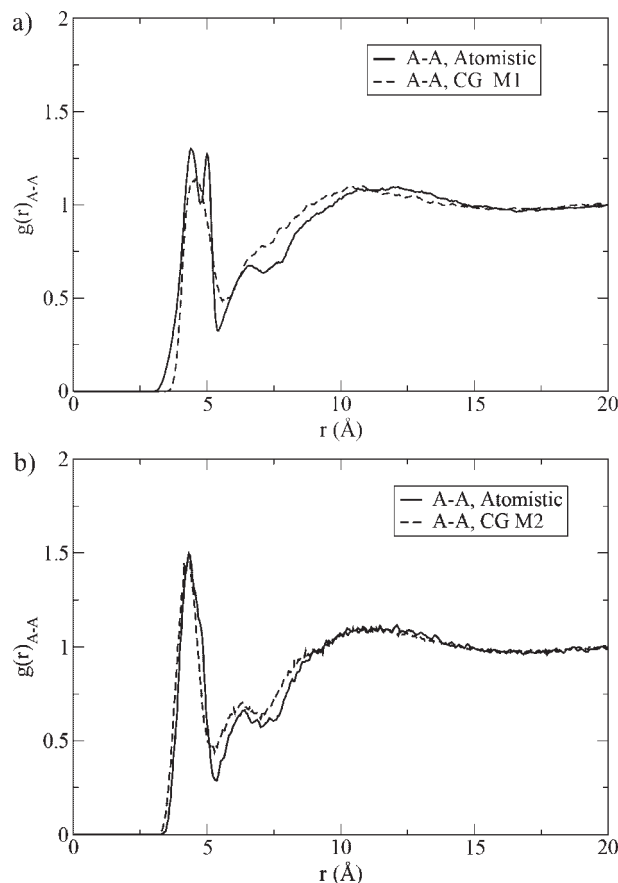


Figure 6. Nonbonded A–A pair distribution function for a PS melt ($MW = 1$ kDa, $T = 463$ K), obtained from atomistic MD (full lines) and CG simulations, analyzed in the two CG mapping schemes: (a) CG M1 and (b) CG M2.

these figures both intra- and intermolecular correlations were taken into account excluding the bonded ones (1–2, 1–3, and 1–4 correlations). Figure 6(a) presents the pair distribution function for the A–A correlations, $g(r)_{A-A}$, obtained from the CG simulations, using the model M1 and from the atomistic data, analyzed at the level of the CG description of M1. The CG data describe correctly the position of the peaks, especially of the first one. However, there are small deviations between the structure of the CG and the atomistic data. In the atomistic data there are two peaks in the short distance up to 5 Å whereas in CG data it is only one and there are small differences even for the larger distances up to around 15 Å. The situation is different for the new mapping scheme. As shown in Figure 6(b), the agreement between the CG data and the atomistic correlations is indeed significantly improved for all distances.

For the B–B correlations the differences are much more pronounced. In Figure 7(a), the results for the CG model M1

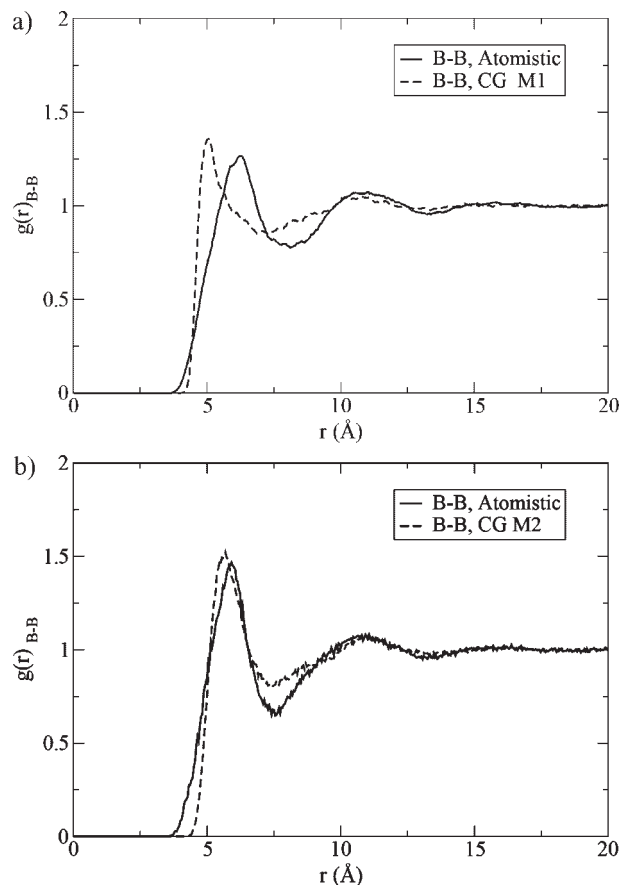


Figure 7. Nonbonded B–B pair distribution function for a PS melt ($MW = 1$ kDa, $T = 463$ K), obtained from atomistic MD (full lines) and CG simulations, analyzed in the two CG mapping schemes: (a) CG M1 and (b) CG M2.

compared to the atomistic simulations are presented. There are some clear deviations, mainly at short distances, up to around 9 Å. First, the position of the first peak from the atomistic data is located at 6.3 Å whereas in the CG simulations it is located at about 5 Å. This smaller distance is a clear indication that the value of σ for the B CG bead (benzene + CH group) is unrealistically small.^a In addition the shape of two curves in Figure 7(a) is rather different, i.e., the curve obtained from the CG runs is much steeper than the atomistic one, proving that the LJ nonbonded interaction between the CG B beads is a too crude approximation. For the larger distances, above 8 Å, the two datasets compare very well. For the new model, M2, [see Figure 7(b)] the situation again improved at all distances; the agreement between the CG and the atomistic data is

^a Results from CG simulations using model M1 with a larger value of σ_B ($=5.3$ Å taken from group contribution methods) shift the position of the first peak to around 5.7 Å.

much better in the short regime (up to 5 Å) and at the same time the agreement at large distances remains.

Overall, the new mapping scheme M2 matches clearly better with the atomistic data. In the new mapping scheme: the new superatoms subsequently lead to softer nonbonded potentials between the CG beads and to a better value of the size of the B CG bead used in the M2 model (which is closer to the real one, compared to model M1). Note that in principle, discrepancies at the level of local packing between the atomistic and the CG description can be expected, as e.g., shown in Figure 6(b) and 7(b). That is in the very nature of the simplification of representing groups of atoms as *spherical* CG beads. Discrepancies are stronger for the B CG bead, which represents a benzene ring in which all atoms are in the same plane. This, however, is not a critical issue as long as reintroduction of the atomistic details in the CG configurations (back-mapping) can be performed without significant disturbance of the CG chains conformations. As we have showed in our previous work,^[12] the back mapping procedure applied to model M1 indeed produces atomistic configurations with local packing in excellent agreement with direct atomistic simulations and experiments. Taking into account, that the new mapping scheme M2 shows even better structural agreement with atomistic data, the back-mapping procedure is even more efficient for the trajectories obtained using the model M2. It should be noted, however, that at lower temperatures, spherical B beads might not reproduce the packing of phenyl rings.

Dynamics

The main advantage of CG simulations is that the time scales accessible by simulations can be greatly increased. Therefore, the speed-up resulting from a specific mapping scheme is a crucial quantity in order to decide which mapping one should choose. The overall speed-up or scale factor, S , of a dynamical mesoscopic simulation, compared to atomistic MD simulations, consists of various contributions, some of which one can calculate precisely.

The speed-up S_{dof} due to the smaller number of degrees of freedom (or particles) in the CG simulations can be easily estimated, as each "superatom" corresponds to n real atoms. Other factors are more difficult to estimate, as they are also interconnected.

The softer nonbonded potentials (energy landscape) result in a reduced effective friction between the beads. The corresponding scale factor S can be estimated from the mean square displacements (MSDs). This can be analyzed in a postprocessing stage. On the algorithmic side, both the softer nonbonded but also the softer bonded potentials allow for a significantly larger time step, leading to another factor S_{dt} . Finally, equilibration issues, or smaller

cutoff distance in the nonbonded interactions (due to using purely repulsive potentials), etc. will influence the performance of a simulation.

As a consequence of the softening of the energy landscape at the mesoscopic description, the time in the dynamic mesoscopic simulations does not correspond to the real time and has to be properly rescaled. Also the question of the smallest length scale on which the dynamics is realistic up to a constant scale factor is certainly of interest. These questions are not new and have already been discussed in the literature (see for example ref.^[6,12,21,29]) in the context of "mapping" the simulation time at the mesoscopic level to data taken either from experiments or from atomistic simulations.

In the following, we try to get an estimation of the scale factor S . Usually, one of the following two methods is used to map the time accurately between the two length scales: the first is to equate a scalar dynamical quantity like the diffusion coefficient or the viscosity. The value for the CG model could thus be matched to the value from detailed atomistic MD runs or experiments. By doing this, only the asymptotic long time regime is being compared. In the case that we have long atomistic MD simulations, an alternative way to map the time is to match the MSD of the chain center of mass (or of the monomers) in the linear regime. Hence, one already compares the time evolution of the MSDs on shorter time and length scales. The time scaling factor determines the real unit to which the CG time corresponds. Because of the universal nature of the polymer motion on scales above a few beads (Rouse regime), this is more appropriate for our study. Thus, we follow the last method by using the data of the atomistic simulations of short PS oligomers.

First, we examine the global chain dynamics. Figure 8 shows the MSDs of chain center of mass, $g_3(t)$, $\{g_3(t) \equiv \langle [R_{\text{cm}}(t) - R_{\text{cm}}(0)]^2 \rangle\}$ of a PS melt (1 kDa, $T = 463$ K) obtained from

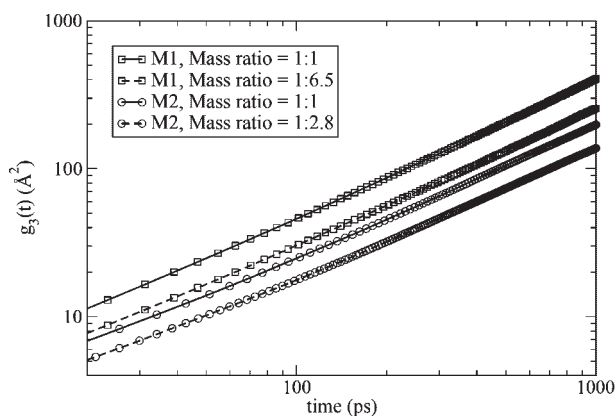


Figure 8. Mean square displacement of the center of mass of PS, obtained from the CG simulations using the two CG models (MW = 1 kDa, $T = 463$ K). The mass ratio corresponds to the mass ratio of the A and B beads (see Figure 1).

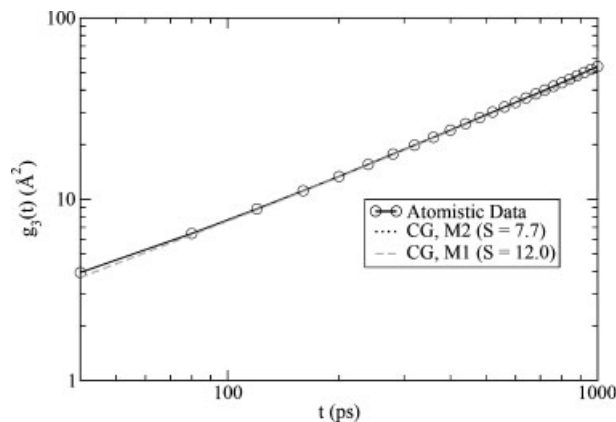


Figure 9. Time mapping, based on the MSD of the center of mass, of the mesoscopic dynamic simulations using atomistic data for a PS melt for the two CG models (MW = 1 kDa, $T = 463$ K).

the two different CG models. As stated above simulations have been done with $m = m_A = 1$, independent of the model used. This allows to set an independent scale. Note that, even though τ has the unit of time, it is the physical time only up to a model specific prefactor. Figure 8 shows four curves, two obtained from CG runs using the assumption that the monomer mass is uniformly distributed, i.e., both CG beads have the same mass (full lines) whereas the other one (dashed lines) are taken from CG simulations where the real mass ratio is assigned to each CG bead. In all cases the curves reach the asymptotic diffusive regime and display a typical short polymer chain behavior.^[23] The data indicate that with uniformly distributed masses, the MSDs are larger, i.e., the effective friction is smaller. The reason probably lies in the discrepancy between the local collision times of the beads for the realistic mass ratios compared to equal masses. Surprisingly, CG runs using the model M1

exhibit faster dynamics than those with the M2 model. This, however, has its reason in the fact that the value of σ_B in model M1 is slightly underestimated due to the way it was originally calculated.

To obtain the true physical time, we now map our CG simulations to our previous united atom simulations, as shown in Figure 8–10. Figure 9 shows the MSDs of the chain center of mass, both for the two different CG models (assuming uniformly distributed mass) as well as from the atomistic runs for a specific system (1 kDa, $T = 463$ K). The CG data (M1 and M2) are indistinguishable, proving that both models describe with the same accuracy the motion of the chain center of mass. Both CG curves follow exactly the atomistic data for distances above only around $8\text{--}10 \text{ \AA}^2$, which is only $1\text{--}2 \sigma^2$, and for times above around 100 ps. The scale factors for the simulation time for the specific system (1 kDa, $T = 463$ K) are $1\tau = 12$ ps for the M1 and $1\tau = 7.7$ ps for the M2 mapping. Note that if data from the CG simulations with the real mass ratios assigned to each CG bead are used, MSDs curves exhibit the same behavior and only the scale factor changes ($1\tau = 4.1$ ps for M1 and $1\tau = 2.7$ ps for M2).

The MSD of the CG beads (averaged over all CG beads) for both CG models as well as the atomistic one (analyzed at the level of the CG description) for a specific system (1 kDa, $T = 463$ K) are presented in Figure 10 and 11. First, the assumption of uniformly distributed mass along the monomer is examined in Figure 10. This figure shows the MSD of CG beads for the new mapping scheme, M2, taken from two runs, one with real masses assigned to each CG bead (dashed line) and one using the same mass for each CG bead (dotted line). Both curves are rescaled in order to match the atomistic data (symbols) in the long time regime by the factor obtained before from $g_3(t)$ matching (see Figure 9). The rescaling factor is, as expected, the same. Both curves show only small differences of each other on

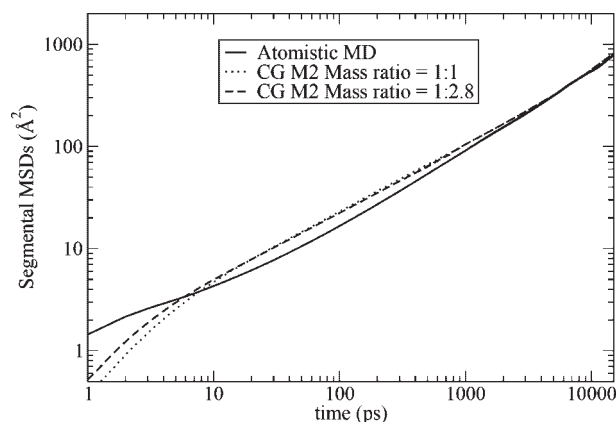


Figure 10. Time mapping, based on the MSD of the CG beads, of the CG dynamic simulations using atomistic data for a PS melt for the new CG model, M2 (MW = 1 kDa, $T = 463$ K).

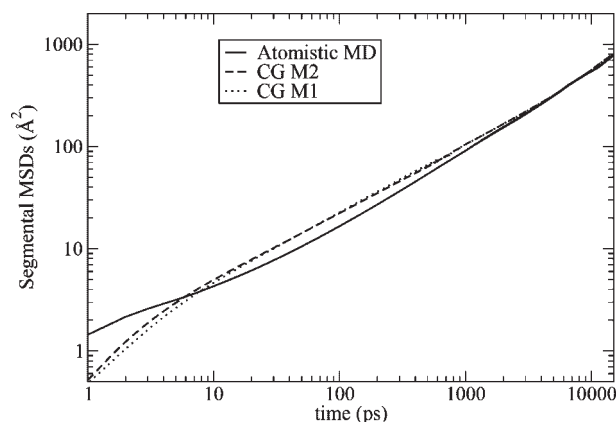


Figure 11. Time mapping, based on the MSD of the CG beads, of the CG dynamic simulations using atomistic data for a PS melt for the two CG models, M1 and M2 (MW = 1 kDa, $T = 463$ K).

Table 3. Time step Δt , used in CG MD simulations and scale factor S for different CG models (1 kDa, $T=463$ K). Note that in atomistic simulations the time step is around 0.001–0.002 ps.

CG model	Δt	S ($1 \tau = S$ ps)
	ps	
M1, $\sigma_B = 4.55 \text{ \AA}$, mass ratio 1:1	0.096	12.0
M1, $\sigma_B = 4.55 \text{ \AA}$, mass ratio 1:6.5	0.035	4.31
M1, $\sigma_B = 5.3 \text{ \AA}$, mass ratio 1:1	0.050	6.25
M1, $\sigma_B = 5.3 \text{ \AA}$, mass ratio 1:6.5	0.015	1.85
M2, mass ratio 1:1	0.077	7.70
M2, mass ratio 1:2.8	0.027	2.70

distances well below 10 \AA^2 and coincide with the atomistic simulations around 100 \AA^2 .

The comparison of the segmental MSDs for the two different CG models is shown in Figure 11. Again both CG curves are rescaled by the factor obtained from Figure 9 in order to match the atomistic data (symbols) in the long time regime. In both cases we show data from runs in which real mass ratios were assigned to each CG bead. Qualitatively the CG data follow the same trend as discussed before.

The major reason for the speedup of M1 being larger than for model M2 originates from slightly smaller bead size σ_B in model M1. Test CG runs using the model M1 with a value of $\sigma_B = 5.3 \text{ \AA}$, taken from group contribution methods as in the new model M2, shows that the CG dynamics becomes around 40% slower. All these results are collected in Table 3. Note that the larger τ , the faster the CG dynamics. If the size (and the excluded volume) of the CG beads is calculated with the same method, then the dynamics of the model M2 is faster than the one for the M1, as one would expect from the analysis of the static correlation functions.

In summary of the discussion above, we can now provide a crude estimate of the overall speed up. For model M2, a time step of around 0.01τ corresponds to a 0.077 ps compared to a time step of around 0.002 ps for united-atom and 0.001 ps for all-atom MD simulations. In our mapping scheme each PS monomer corresponds to two CG beads compared to is eight (united-atom) or 16 (all-atom). As an example, a brute force united-atom MD run of a low MW ($= 1$ kDa) PS melt with a rather small system (45 chains), needs around 50 d using a Power 4 (1.7 GHz) processor, whereas the CG run with a system more than ten times larger (480 chains) needs less than 1 d, giving a speedup of around 500. For an all atom simulation this scales up to about 2 000. In addition, equilibration of the polymer chains in the CG description is much faster compared to the atomistic one.

Conclusion

We have presented a detailed investigation of two CG mapping schemes for PS and show how relatively small changes influence the performance of the models. Both CG models were chosen such that each PS monomer is represented by two CG beads (2:1 model). In the first model M1, the CH_2 group of the backbone chain represents one effective CG bead (type A), whereas the remaining CH group of the monomer in the backbone and the phenyl ring are mapped into another effective CG bead (type B). In the new mapping scheme M2, CG bead A comprises of the CH_2 of a PS monomer plus the half mass of each one of the two neighboring CH groups along the chain backbone, whereas CG bead B corresponds to the phenyl ring. This difference in choice has significant consequences for the results of the CG simulations.

The proposed mesoscopic models have been tested and compared along a different number of properties. Conformations of short PS chains at the monomeric level (distribution function of bonds, bending and dihedral angles) as well as on the level of the whole chain (internal distances, radius of gyration, end-to-end distance) were found in good agreement between the two CG mapping schemes and also with the ones obtained by atomistic MD runs. However, the new mapping scheme M2 describes the $(\theta-\phi)$ correlations more accurately.

More significant differences in the two models were found for the melt structure. By means of softer non-bonded repulsive potentials and beads closer in size, the bead pair distribution functions in the melt are described better with the new model.

The segmental – as well as the chain – dynamics has been compared with detailed atomistic data by using a proper time mapping based on MSDs of short PS chains. Both CG models describe very well the chain dynamics for distances only above around 10 \AA^2 , roughly the size of a monomer, and for times above around 100 ps. The overall

speed-up turns out to be ≈ 2000 compared to all-atom MD and ≈ 500 compared to united-atom simulations, respectively. This allows for much larger systems and significantly longer times in future simulation studies of PS.

Acknowledgements: The authors thank *Christine Peter* for many useful discussions and comments on the manuscript.

Received: May 3, 2007; Revised: June 25, 2007; Accepted: June 27, 2007; DOI: 10.1002/macp.200700245

Keywords: polystyrene; structure

- [1] "Monte Carlo and Molecular Dynamics Simulations in Polymer Science", K. Binder, Ed., Oxford University Press, New York 1995.
- [2] J. D. Ferry, "Viscoelastic Properties of Polymers", John Wiley and Sons, New York 1980.
- [3] J. Baschnagel, K. Binder, P. Doruker, A. A. Gusev, O. Hahn, K. Kremer, W. L. Mattice, F. Müller-Plathe, M. Murat, W. Paul, S. Santos, U. W. Suter, V. Tries, *Adv. Polym. Sci.* **2000**, *152*, 41.
- [4] K. Kremer, F. Müller-Plathe, *MRS Bull.* **2001**, *26*, 205.
- [5] K. Kremer, *Proceedings of the International School of Solid State Physics – 34th Course: Computer Simulations in Condensed Matter: From Materials to Chemical Biology*, K. Binder, G. Ciccoti, Eds., Erice 2006.
- [6] W. Tschöp, K. Kremer, J. Batoulis, T. Buerger, O. Hahn, *Acta Polym.* **1998**, *49*, 61.
- [7] C. Abrams, K. Kremer, *Macromolecules* **2003**, *36*, 260.
- [8] D. Reith, M. Pütz, F. Müller-Plathe, *J. Comp. Chem.* **2003**, *24*, 1624.
- [9] D. Reith, H. Meyer, F. Müller-Plathe, *Macromolecules* **2001**, *34*, 2335.
- [10] H. Meyer, O. Biermann, R. Faller, D. Reith, F. Müller-Plathe, *J. Chem. Phys.* **2000**, *113*, 6264.
- [11] H. Fukunaga, J. Takimoto, M. Doi, *J. Chem. Phys.* **2003**, *116*, 8183.
- [12] V. A. Harmandaris, N. P. Adhikari, N. F. A. van der Vegt, K. Kremer, *Macromolecules* **2006**, *39*, 6708.
- [13] G. Milano, F. Müller-Plathe, *J. Phys. Chem. B* **2005**, *109*, 18609.
- [14] Q. Sun, R. Faller, *Macromolecules* **2006**, *39*, 812.
- [15] Q. Sun, R. Faller, *Comp. Chem. Eng.* **2005**, *29*, 2380.
- [16] T. Spyriouni, C. Tzoumanekas, D. N. Theodorou, F. Müller-Plathe, G. Milano, *Macromolecules* **2007**, *40*, 3876.
- [17] G. Santagelo, A. di Matteo, F. Müller-Plathe, G. Milano, *J. Phys. Chem. B* **2007**, *111*, 2765.
- [18] W. L. Mattice, Y. B. Tatek, N. Waheed, *Macromolecules* **2007**, *40*, 379.
- [19] X. J. Li, D. Z. Kou, S. L. Rao, H. Liang, *J. Chem. Phys.* **2006**, *124*, 204909.
- [20] J. Padding, W. J. Briels, *J. Chem. Phys.* **2002**, *117*, 925.
- [21] S. J. Marrink, A. H. de Vries, A. E. Mark, *J. Phys. Chem. B* **2004**, *108*, 750.
- [22] V. A. Harmandaris, N. P. Adhikari, N. F. A. van der Vegt, K. Kremer, B. A. Mann, R. Voelkel, H. Weiss, C. C. Liew, *Macromolecules* in press.
- [23] K. Kremer, G. Grest, *J. Chem. Phys.* **1990**, *92*, 5057.
- [24] A. Bondi, *J. Phys. Chem.* **1964**, *68*, 441.
- [25] R. Auhl, R. Everaers, G. S. Grest, K. Kremer, S. J. Plimpton, *J. Chem. Phys.* **2003**, *119*, 12718.
- [26] J. Mark, K. Ngai, W. Graessley, L. Mandelkern, E. Samulski, J. Koenig, G. Wignall, "Physical Properties of Polymers", 3rd edition, Cambridge University Press, Cambridge 2003.
- [27] H. J. Limbach, A. Arnold, B. A. Mann, C. Holm, *Comput. Phys. Commun.* **2006**, *174*, 704; see also: <http://www.espresso.mpg.de/>.
- [28] C. D. Wick, M. G. Martin, J. I. Siepmann, *J. Phys. Chem. B* **2000**, *104*, 8008.
- [29] B. Hess, N. F. A. van der Vegt, K. Kremer, *Soft Matter* **2006**, *2*, 409.